DEMONSTRATION OF VIRTUAL MIMO IN THE UPLINK

V. Jungnickel*, M. Schellmann*, A. Forck*, H. Gäbler*, S. Wahls*, A. Ibing*, K. Manolakis*
T. Haustein[×], W. Zirwas[×] J. Eichinger[×], E. Schulz[×], C. Juchems[†], F. Luhn[†], R. Zavrtak[†]

*Fraunhofer Institute Telecommunications, Heinrich-Hertz-Institut, Einsteinufer 37, D-10587 Berlin, Germany
[×]Nokia Siemens Networks GmbH & Co. KG, Werinherstrasse 91, D-81541 München, Germany
[†]IAF GmbH, Berliner Strasse 52J, D-38104 Braunschweig, Germany

(invited paper)

Keywords: Multiuser detection, SDMA, MIMO, remote synchronization, real-time implementation.

Abstract

We demonstrate how virtual MIMO techniques can be implemented in a next-generation mobile communication system. In order to test basic principles, joint spatiotemporal processing of two users has been implemented in an uplink scenario. A prerequisite of virtual MIMO is accurate synchronization. It is shown that the carrier frequency offset can be reduced to a few Hz only at small signal-to-noise ratios. Based on remote synchronization via the downlink, a technique called frequency advance is applied in the uplink, i.e. the terminals correct their frequency offsets in the digital baseband prior to data transmission. The principle has been implemented and tested in real-time using system parameters of the long term evolution (LTE) of the 3rd generation (3G) of cellular systems. Two user's signals have been successfully detected on the same radio resource.

1 Introduction

The buzzword virtual MIMO denotes a certain class of spatiotemporal processing techniques in which the classical multiple-input multiple-output (MIMO) transmission schemes are further developed using some kind of coherent cooperation between distributed radio nodes. The best-known application is cooperative diversity (Fig. 1, top). Multiple mobile nodes are synchronized remotely and interact coherently to support advanced communication protocols.
The principle of virtual MIMO is that at transmitting, receiving, or at both sides of the link, spatiotemporal processing is utilized in order to increase the capacity. Significant gains in spectral efficiency are predicted in this way, similar to classical MIMO systems described in [1], [2].
The area of virtual MIMO is extensively explored in research towards wireless networks with multiple nodes in multi-hop configurations. The reader is referred to the literature on cooperative diversity, for an overview see [3].
However, the remote synchronization needed for virtual MIMO is rarely considered in the literature. It is shown in [4] that timing errors may have similar effects as inter-symbol interference (ISI). The impact of carrier frequency offsets (CFO) is studied in [5], where a Viterbi equalizer is proposed to realize a graceful degradation.

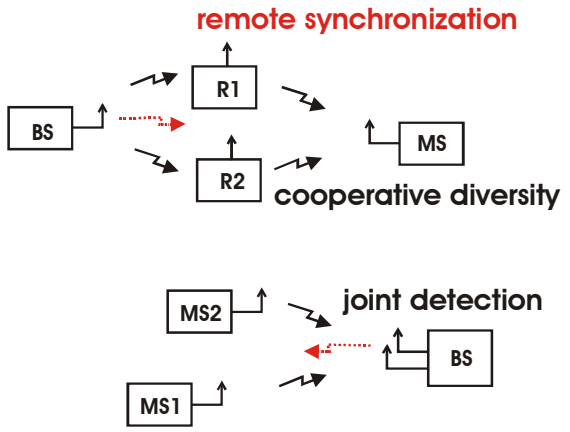

Fig. 1: Two examples of virtual MIMO. Remote synchronisation is always required.

Next-generation cellular communication systems are based on orthogonal frequency-division multiplexing (OFDM). It is interesting to note that the classical multiple access channel in OFDM based multi-antenna systems, i.e. the spatiotemporal detection of multiple users at a base station, includes a similar remote synchronization problem as virtual MIMO (see Fig. 1, bottom).
The detailed analysis in [6] has shown that individual user's CFOs violate the cyclostationary properties of the OFDM uplink channel. As a result, there is a crucial interference after joint spatial processing on each OFDM subcarrier and subsequent individual carrier phase tracking for each user. A fundamental insight from this analysis is that the *CFOs must be kept very small already at the terminal sides* in order to realize multi-antenna joint detection in the uplink.
Accordingly, we propose a remote synchronization procedure denoted as frequency advance in this paper, where the terminals perform fine synchronization via the downlink and correct their individual CFO in the digital baseband prior to the uplink transmission. The basic idea is implemented in real time using system parameters close to 3G LTE. Joint detection has been tested over the air under typical laboratory conditions.
The paper is organized as follows. Parameters of the experimental system are listed in section 2. Section 3 describes the principle of frequency advance. Section 4 considers channel estimation and interpolation.

Implementation of the MMSE equalizer is described in section 5. Section 6 considers the DFT pre-coding in the uplink, which is a particular requirement in LTE. System integration is reported in section 7. The demonstration setup and results are described in section 8.

2 Experimental system parameters

System parameters used in our experimental LTE system are listed in table 1. Prototype development has started at the end of 2005. Hence, parameters reflect early LTE working assumptions and may not be identical to the final standard. Nonetheless, they are still representative for the LTE system.

3 Frequency advance

3.1 Downlink synchronization

In the first downlink TTI in each radio frame, no data but two preambles are transmitted. The structure is shown in Fig. 2. Symbols are constructed using a 512-point FFT, where only each 4th sub-carrier is used. While the B-part uses carriers No. ±4, ±8, ±12, …, and zero carrier is not used, the A-part uses carriers No. ±2, ±6, ±10, …. Due to the shift in frequency domain, signs of periods are altered. Each symbol is extended by appending the last 128 samples again. Note that carriers outside the variable system bandwidth (1.25, 5, 10, 20 MHz) are set to zero. Such a variable-bandwidth preamble guarantees a smaller timing jitter and a higher probability of detection in frequency-selective fading channels. In more recent LTE specifications, a narrow-band preamble is used [7]. Performance is compared in [8].

Beginning of frame (BOF) and CFO are coarsely estimated using the well-known Schmidl-Cox autocorrelation circuit (SC in Fig. 3) [9], [10]. Since the preamble is much longer than in wireless LANs based on the IEEE 802.11g standard, coarse synchronization works fine also at low signal-to-noise ratios (SNR) typical for cellular systems. At an SNR of 0 dB and with 20 MHz bandwidth, in 90% of cases the BOF jitters by not more than one sample (≈3 ns) in AWGN channel.

After coarse CFO estimation, the standard deviation at 0 dB SNR is roughly 100 Hz in AWGN channel, consistent with theory [10, 11]. Therefore, a fine synchronization loop as proposed in [12] has been implemented (see Fig. 3). To simplify implementation, 12 orthogonal pilot tones per antenna have been embedded between resource units in our experimental system, similar as in 802.11g (see Fig.5). After channel equalization (using maximum ratio combining at 2 receive antennas), the common phase error (CPE) and the phase error due to the sampling clock offset are estimated from pilot tones. The CPE is fed back through a finite impulse response (FIR) loop filter to a compensation circuit in front of the FFT (see Fig. 3) which works as follows: At the start of the next TTI, the residual frequency error obtained from the CPE is added to the previous CFO such that the previous value is improved. The oscillation with opposite phase compared to the downlink CFO is created in a direct digital synthesizer (DDS) and multiplied with the received signals in order to reduce the CFO in the baseband signal.

downlink/uplink, full duplex	2.53/2.68 GHz
antennas base station/terminal	2 TRx/2 TRx
Sampling rate	30.72 MHz
used bandwidth	Up to 18 MHz
symbol period downlink /uplink long (short) block	71.4/70.1 (37.5) ns
cyclic prefix downlink/uplink	4.6875/4.13 ns
total number of sub-carriers	2.048
number of used sub-carriers	up to 1.200
transmission scheme downlink	OFDMA BLAST
modulation in downlink	4-,16-,64-QAM
transmission scheme uplink	SC-FDMA CDD
modulation in uplink	2-, 4-, 16-, 64-QAM
radio frame	10 ms
transmit-time interval (TTI)	0.5 ms
symbols/TTI in downlink	7
symbols/TTI in uplink	6 long, 2 short
resource block size	25 carriers in 1 TTI
channel coding	Convolutional
code rates	½, ¾

Table 1: Parameters of the experimental LTE system.

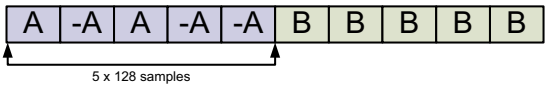

Fig. 2: Preamble used for coarse synchronization.

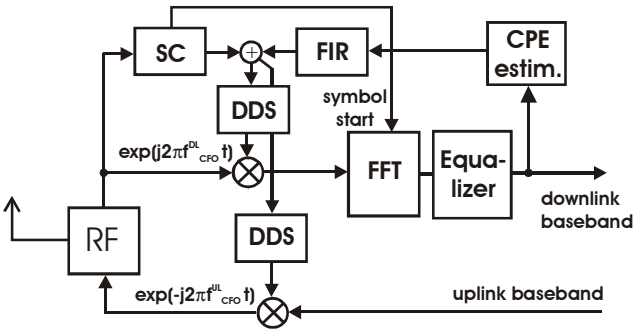

Fig. 3: Principle of frequency advance.[1]

In Fig. 4, the dependency of the CFO on SNR is shown for tow cases: The implemented system and the current status of the LTE standardization [7]. It can be observed that the coarse CFO estimation in the experimental system works better than in the standard proposal, due to the wider bandwidth of our preamble. Vice versa, the fine synchronization in the demonstrator is worse than in the standard proposal. The origin is the relatively small number of phase tracking pilots used in the demonstration system for the CPE estimation. If the energy of all pilots available for the channel estimation is also exploited in the CPE estimation, a better performance can be achieved. Altogether, at 0 dB SNR, residual CFOs of a few Hz are feasible based on LTE.

[1] SC: Schmidl-Cox correlation, DDS: Direct digital synthesizer, FIR: Finite impulse response filter, CE: Channel estimation, CPE: Common phase error, RF: Radio front-end, FFT: Fast Fourier transform.

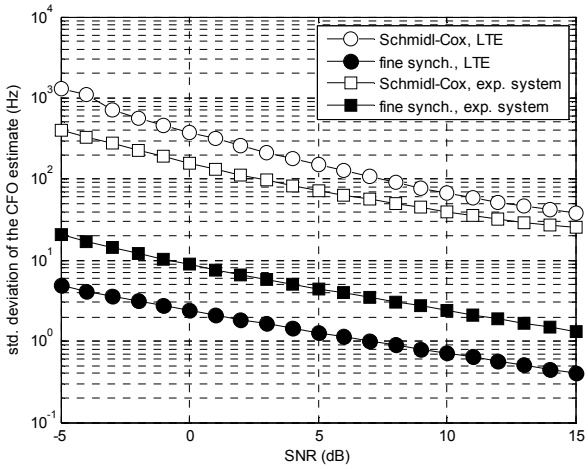

Fig. 4: Results for coarse and fine CFO synchronization.

3.2 Uplink synchronization

In the frequency advance technique, uplink synchronization is closely related to the downlink. Notice that local oscillators (LO) of transmitter and receiver front-ends in frequency-division duplex (FDD) modems do have different frequencies. Both LOs are normally coupled to a common low-frequency reference oscillator having the frequency f_{ref}. In fact, the CFO is directly related to the frequency difference Δf_{ref} of the two reference oscillators at the base station and terminal sides. The phase locked loops (PLL) coupling the LOs to these references typically include factors N and M that are integers or fractions of integers (e.g. a factor of 268 with 10 MHz reference at 2.68 GHz carrier frequency). Hence, the downlink frequency can be written as $f_{CFO}^{down} = N\Delta f_{ref}$ and uplink frequency as $f_{CFO}^{up} = -M\Delta f_{ref}$, where N *and* M are not equal in FDD mode. Obviously, since

$$f_{CFO}^{up} = -\frac{M}{N} f_{CFO}^{down}, \qquad (1)$$

up- and downlink CFOs are strictly coupled. For frequency advance, we have estimated the CFO in the downlink using the fine synchronization described above. From the result, we obtained the uplink CFO according to (1). Similarly as in the downlink receiver chain, the opposite phase oscillation was created in a second DDS (see Fig. 3). The uplink baseband signal was then pre-compensated at each terminal individually for the individual uplink CFO. The signals of different terminals arrive without significant frequency offset at the base station. The residual offset between different remote nodes is similar to a Doppler spread of the incoming signals. Mobile communication systems are robust to Doppler spreads, due to the use of short coherence intervals where the channel is considered constant.

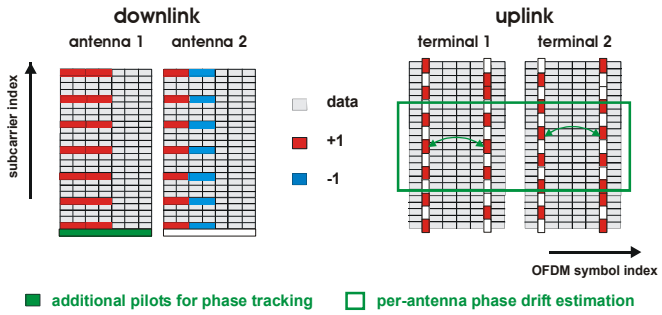

Fig. 5: Local downlink (left) and uplink (right) pilot grids.

4. Channel estimation

High-quality channel estimation for 3G LTE is a challenge in real time. Pilots are available only on a sparse grid in the time-frequency domain. On intermediate subcarriers and time slots, one must use channel interpolation. Since all users can listen to all pilots in the downlink, the optimal solution is to use all pilots for interpolation. However, this is impractical with current digital signal processors (DSP).

For example, in order to interpolate the LTE channel in 20 MHz bandwidth, one needs 1.200 channel coefficients for each pair of transmit and receive antennas from each 4th sub-carrier being a pilot. For the optimal Wiener filter, we have to compute an interpolation matrix of size 1.200x300, which includes the inversion of a 300x300 matrix. Next we multiply the interpolation matrix with a vector of size 300x1 containing received pilots. Complexity of matrix inversion is given as $300^3 = 2.7 \cdot 10^7$, fortunately these matrices can be pre-computed. The matrix-vector multiplication complexity of $1200 \cdot 300 = 3.6 \cdot 10^5$ must be realized in real time. If a TTI with 0.5 ms duration is considered as coherence interval, and 4 times this complexity is needed in a 2x2 MIMO system, we end up with roughly $4 \cdot 10^9$ real-valued multiplications per second. This number would exceed the processing power of current DSPs, and hence interpolation has been simplified.

Local interpolation has been used instead. It relies on a subset of pilots in the local area around the desired resource unit. A decision-aided technique reported in [13] provides better performance at high SNR. But linear techniques perform better at low SNR typical for cellular radio. In [14], it is shown that one must sacrifice only a small fraction of the interpolation gain to reduce the computational burden by a factor of 20 based on local interpolation. Prerequisite for this is a sophisticated SNR estimation which makes the filter more robust. For the power delay profile, a favourable assumption is to use an exponential profile with decay time equal to half of the cyclic prefix length (see [14]).

We have implemented the local interpolation as described in [14] on a Texas Instruments (TI) 6713 DSP operating at 300 MHz clock. Local interpolation is applied separately in each resource unit which spans 25 subcarriers times 7 OFDM symbols, for each pair of transmit and receive antennas. Implementation is simplified by the common WSSUS[2]

[2] **w**ide-**s**ense **s**tationary **u**ncorrelated **s**cattering

assumption. Interpolation matrices are independent of frequency when the local pilot grids are identical. This point has been regarded when defining the pilot patterns inside the resource units described below. We have stored pre-computed filter matrices according to the estimated SNR. Runtime of local interpolation (which has been applied step-wise over the entire 20 MHz LTE band) is about 0.1 ms. This time is well within our 0.5 ms coherence interval.

4.1. Downlink pilots

Our local downlink pilot grid is shown in Fig. 5 (left) for a single resource unit on both antennas. A code-multiplexed approach is used along the time axis and each 4th subcarrier is used. By this spacing, pilots are placed at the edges of resource units which reduce the interpolation error. Antennas are identified by sequences with a length of 4 along the time axis taken from an orthogonal set. Additional scrambling is applied along the frequency axis. Correlation over multiple OFDM symbols along the time axes [15] is applied prior to interpolation along the frequency axes, which is carried out individually for each pair of transmit and receive antennas.

4.2. Uplink pilots

Our uplink resource unit comprises 6 long blocks (LB, i.e. OFDM symbols with 2048 subcarriers) and 2 short blocks (SB, i.e. OFDM symbols with 1024 subcarriers). Pilots are located within the SBs, see Fig. 5, right. Each terminal is identified by a pilot sequence using disjoint sets of subcarriers within the SB. Time- and frequency interpolation are carried out separately. In the time domain, possible amplitude variations have been ignored. The mean phase drift $\Delta\phi$ is evaluated for each terminal based on the pilots inside the rectangle indicated in Fig. 5. Raw estimates H are averaged as

$$H = \frac{1}{2}\left(H^{SB1} + H^{SB2} \cdot e^{-j\Delta\phi}\right) \qquad (2)$$

to reduce the effects of noise. Frequency-domain interpolation in uplink exploits the fact that the coefficient measured at a given pilot carrier i in a SB corresponds to the carrier with index $2 \cdot i$ in a LB. The odd number of 25 carriers caused overlap at the edges of resource units (see Fig. 5, right). We have performed local interpolation over two adjacent resource units, accordingly. While the channel estimates are used to compute weight matrices for multiuser detection, the phase values are passed to the tracking unit placed after the multiuser detector. Phase tracking has been operated at frequency $\Delta\phi/(4.5 \cdot T_{LB})$, where T_{LB} is the LB duration.

5. MMSE equalizer

The implementation is partitioned between FGPA and DSP as indicated in Fig. 6. While the equalization is done in the FPGA, weight matrix calculation is done in DSPs.

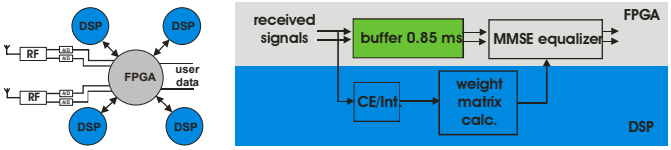

Fig. 6: Principal partitioning of signal processing.

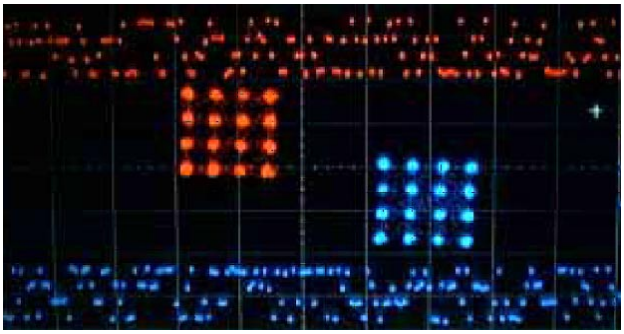

Fig. 7: Despite frequency advance, there is a small residual frequency offset after the user separation at the base station. It is removed by additional phase tracking.

The most challenging tasks for real time implementation is the weight matrix computation. In a preceding 1 Gbit/s trial with a 3x5 antenna configuration and 64 subcarriers [15, 16], one TI 6713 DSP was used to obtain all weight matrices within 2 ms. For LTE, in comparison, the number of subcarriers is increased by factor 32 while only a 2x2 antenna configuration has been implemented. Complexity of weight calculation scales linearly with number of carriers but cubically with the number of antennas at one side of the link. We can say that the complexity per coherence interval is roughly increased by factor 4 compared to [15].

Signal processing has been divided among 4 TI 6713 DSPs (Fig. 6, left) each of which is connected over an individual bus to the FPGA. Each DSP is responsible for 300 carriers. It is synchronously operated in a loop with a period of 0.5 ms, according to the TTI duration. The complexity has been further reduced to realize such a short period: Customized routines for multiplication of small matrices provided by TI have been used for the MMSE equalizer weight calculation. Complex-valued calculation is always utilized. For the matrix inversion being part of the MMSE weight calculation, a closed-form expression of the inverse 2x2 matrix is used instead of Gauss-Jordan. This is less complex for 2 transmit and 2 receive antennas. For the noise variance needed in the MMSE equalizer, we have used the estimated values from the channel interpolation routine described in section 4.

Altogether, reading coarse channel estimates into the DSP, performing channel interpolation and MMSE weight matrix calculation and writing weight matrices back into the FPGA is done in about 0.3 ms in downlink and 0.45 ms in uplink where additional phase estimation is extracted from the pilots.

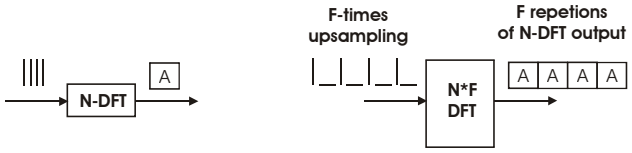

Fig. 8: A DFT with variable size can be realized by up-sampling using a fixed-size DFT.

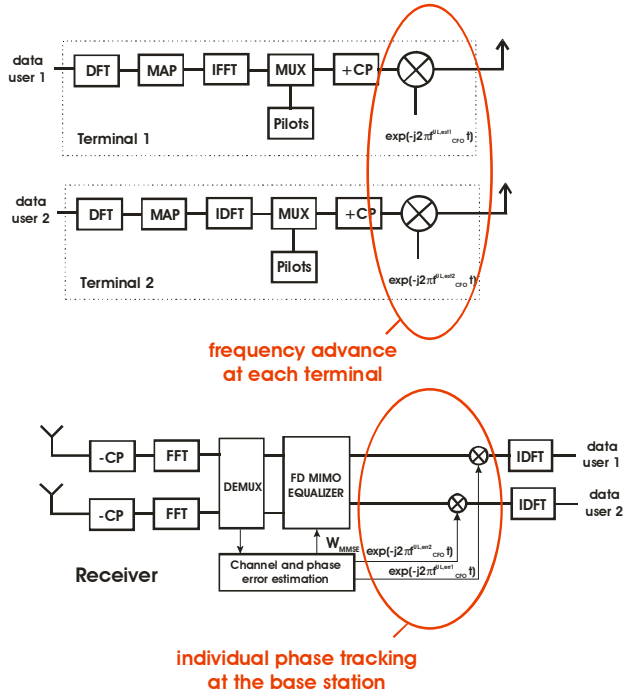

Fig. 9: Uplink transmitters and receiver for virtual MIMO.

The equalization is implemented in the FPGA as described in [16]. It uses a pipelined matrix-vector multiplication where multiple on-chip multipliers are operated in parallel and weight matrices are exchanged from one subcarrier to the next. The stream of received signals is buffered after FFT for altogether 12 OFDM symbol durations, before entering the equalizer (see Fig. 6, right). In this way, weight matrices arrive time-aligned with received signals. The buffer consumes 90 kByte on-chip memory. This buffering allows a higher mobility but time for buffering (≈0.85 ms) must be regarded when latency is evaluated.

Despite the frequency advance, there is an inevitable phase offset at each terminal which is assigned to the residual estimation error for the downlink CFO. Fig. 7 shows the residual phase rotation of received constellation diagrams visualized directly after the MMSE equalizer in the frequency domain. In our test case, both terminals have mapped 16-QAM data signals directly onto the inner OFDM transmitter (i.e. without DFT pre-coding described in section 6). While top and bottom traces in Fig. 7 show I_1 and Q_2 signals of the first and second terminal (subcarrier index on horizontal axes), respectively, the 16-QAM constellations are rotated by less than 5° for each terminal at the receiver. Based on the 0.5 ms lag in the fine synchronization loop at the terminal, we can estimate that the residual CFO is smaller than 5°/0.5 ms≈3 Hz under laboratory conditions, at an SNR of approximately 10-15 dB. This is consistent with simulation results in Fig. 4.

The residual phase drift is a random process which must be corrected instantaneously at the base station, individually for each terminal. As mentioned in section 4, the residual offset is evaluated as a part of the uplink channel estimation procedure in the base station. The offset values are delivered from the DSPs to the FPGA where they are corrected out of the user signals immediately after the MMSE detector (see Fig. 9).

6. DFT precoding

DFT pre-coded OFDM is a particular kind of single-carrier transmission with cyclic prefix (CP) introduced in LTE for two major reasons. Firstly, single-carrier transmission reduces the power fluctuations of the output waveforms at the transmitter and allows a better usage of the power amplifier. Secondly, the DFT pre-coding spreads the information across the assigned set of subcarriers and thus enables the use of multipath diversity.

Currently available DFT cores for FPGAs have a fixed number of points [17, 18].[3] In order to realize a variable bandwidth, one must be able to change the number of points at run time.

Such a variable DFT with a selectable number of points has been realized with variable up-sampling in front of a custom-made 1.200 point DFT (see Fig. 8). In order to realize our variable DFT of size N=1.200/F, where F is an integer, the input signal is F-times up-sampled with F-1 zeros inserted in between input values. This yields F periodic blocks after the 1.200-point DFT, where each block is identical to the desired N-point DFT output. One of these blocks is further processed, mapped to the desired resources and fed into the IFFT of the OFDM transmitter. This solution lacks flexibility and it is more complex than a variable DFT. At the time of writing, there has been no flexible FPGA-based DFT implementation available. Note that even multiuser multiplexing is feasible with this approach [19].

Care must be taken with the scaling after the DFT, before the signal is fed into the inner OFDM transmitter. At first, the output must be scaled depending on bandwidth used. Signals are fed with same mean amplitude per carrier into the IFFT. Furthermore, signals must be decimated properly after the DFT output, which is divided by a number representing the occupied bandwidth. We have used divisors 300, 150, 75 and 19 to realize a variable bandwidth of 20, 10, 5, and 1.25 MHz, respectively.

Note that there are significant power fluctuations in the waveforms despite the DFT pre-coding. This can be improved by raised cosine filtering as suggested in [20]. However, it has not been applied here.

[3] The fixed size 1.200 point DFT soft core needs as many resources in the FPGA as four 2.048 point FFT cores.

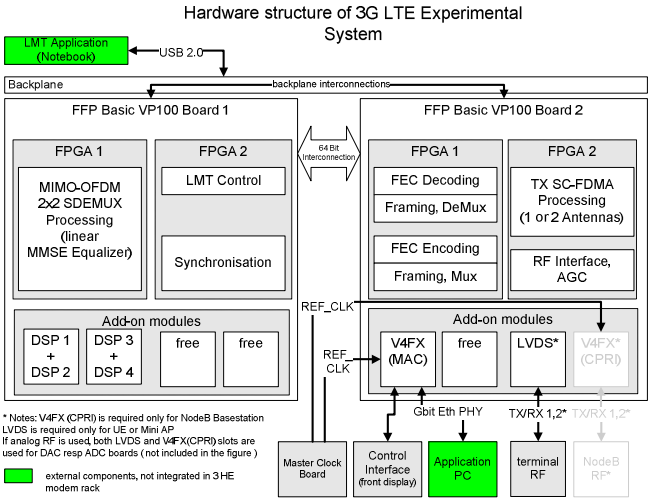

Fig. 10: Functional mapping at the terminal side.

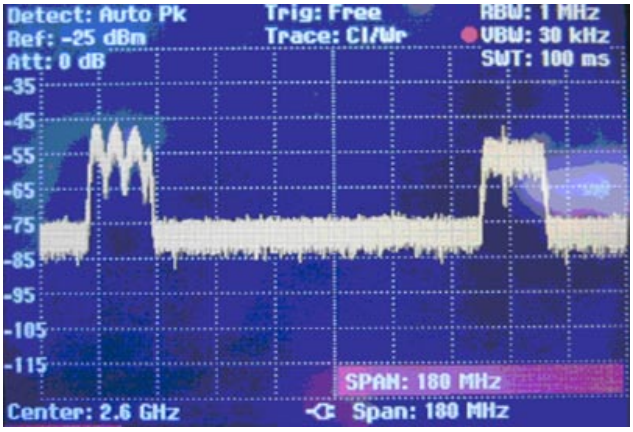

Fig. 11: Uplink (left) and downlink (right) spectrum on air.

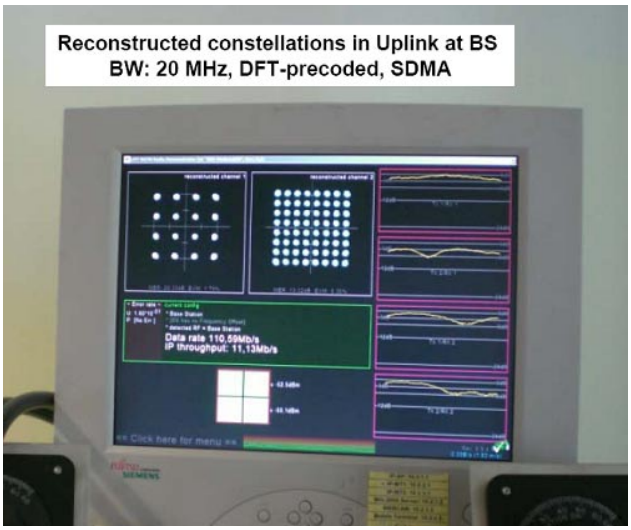

Fig. 12: Separated user constellations (left) and channel coefficients from the two terminals to the two base station antennas, displayed on the monitoring terminal.

7. System integration

The complete physical layer for the joint detection of 2 users with a base station using 2 antennas is summarized in Fig. 9. At the terminal side, it comprises the DFT pre-coding, mapping to resource units, IFFT, multiplexing with pilots, adding the CP, and the frequency advance, based on the fine synchronization in the downlink. At the base station side, after removal of the CP and FFT, pilots are separated, the channel is estimated and interpolated and the residual phase drift is obtained. The equalizer weight matrices $\mathbf{W}_{MMSE}$ are computed for each subcarrier and the users are separated in the frequency domain using the linear MMSE equalizer. Finally, the phase drift due to the residual fine frequency estimation error in the downlink is individually corrected for each terminal signal and the data signals are recovered after the IDFT.

The physical layer of one LTE transceiver is implemented on 2 *FFP basic* motherboards each containing 2 Virtex2Pro/100 FPGAs. At the receiver, both in uplink and downlink direction, four TI 6713 DSPs are used for channel interpolation and equalizer weight matrix calculations.

FPGAs operate at 30.72 MHz clock. The functional mapping on hardware is sketched in Fig. 10 at the terminal side. Framing and forward error encoding (FEC) in the uplink direction as well as decoding and de-mapping for the downlink direction are hosted in the left FPGA on board 2. The right FPGA on board 2 hosts the transmit processing for the uplink as well as the interfaces to the RF unit. The left FPGA on board 1 contains the MIMO-OFDM MMSE equalizer for the downlink. Coarse and fine synchronization in downlink are implemented in the right FPGA on board 1. In total four DSPs are mounted in a sandwich-like fashion on board 1 as well (see Fig. 10).

There are external interfaces to the RF frontends, to 1 Gbit/s Ethernet for real-time data applications, and to the local monitoring terminal (LMT) where received constellations, channel estimates and other information are displayed.

Terminal RF units operate in full-duplex FDD mode at 2.53 and 2.68 GHz. The spectrum on the air is shown in Fig. 11. Note that the second transmitter, which is available in our experimental terminals, has been fed with the same signal and cyclic delay diversity has been applied. This is the origin of the notches in the uplink spectrum. At the base station, commercial RF units and duplex filters matched to the new 3G spectrum have been used. As indicated in Fig. 10, terminal and base station RF frontends are digitally coupled via parallel cable using low-voltage differential signalling (LVDS) and serial 1.2 Gbps common public radio interface (CPRI), respectively.

8. Demonstration of virtual MIMO

The demonstration has been conducted in a large laboratory room of 20m x 8m x 3 m size. The room has three doors at each side and a window front on the 4th side and it contained typical office furniture (e.g. chairs, tables with computers). The base station was located in a corner of the room. The two terminals were placed statically about 6 or 8 m away from the

base station at positions where their signals were received with approximately equal power. About 30 people were in the room. As a consequence, the channel was varying over time. The base station and both terminals were equipped with cross-polarized indoor antennas.

In Fig. 12, the separated constellations of terminal 1 (left) and terminal 2 (centre) are shown. At the right hand side, the channel frequency responses between the two terminals and two receive antennas at the base station are shown. Being typical for indoors, there is little frequency-selective fading in the 20 MHz system bandwidth. During this screenshot, terminal 1 has transmitted an 11 Mbit/s high-resolution HDTV video stream via the internet protocol (IP), using 16-QAM modulation, while terminal 2 transmitted pseudo-random data in 64-QAM format. In downlink direction, both terminals received a 30 Mbit/s high-resolution HDTV video.

Most strikingly, the mutual cross-talk between both terminal signals, which results at the base station after transmitting them simultaneously over the air, has been almost completely removed in real time by the linear MMSE detector operating in the frequency domain, such that after IDFT and FEC, the data are detected free of errors.

Conclusions

To the best of the author's knowledge, spatiotemporal multiuser detection using an antenna array at the base station (alias space-division multiple access, SDMA, or virtual MIMO) has been demonstrated for the first time over the air for a next-generation cellular communication system based on OFDM. For the realization, terminals have used orthogonal pilots. Moreover, a technique called frequency advance has been applied for remote synchronization over the downlink. The carrier frequency offset is corrected in the digital baseband at the terminal side prior to the uplink transmission.

In this way, the impact of inter-carrier interference can indeed be minimized and excellent spatiotemporal user separation becomes feasible. The residual carrier frequency offset has been reduced down to a few Hz typically, and this rest has been corrected at the base station by individual carrier phase tracking for each terminal. Error free data transmission for two terminals using 16- and 64-QAM modulation has been demonstrated in a typical indoor scenario.

Since the residual CFO in transmit direction is so small, the common assumption that remote nodes transmit coherently in virtual MIMO deployments may be justified in practice. In the framework of new cellular radio, novel techniques will be feasible, as cooperative relaying and multi-hop wireless networking between the base stations. Future work concerns the space-frequency adaptive multiuser scheduling in the medium access control (MAC) layer, and the measurement of achievable throughput gains using SDMA.

Acknowledgements

The work reported in this paper has been conducted in the collaborative research project "3G evolving technologies (3GeT)". Financial support by the German Federal Ministry of Education and Research (BMBF) is acknowledged.

References

[1] E. Telatar, "Capacity of multi-antenna Gaussian channels," *Europ. Trans. Telecom.*, Vol. 10, No. 6, Nov.-Dec. 1999, pp. 585-595.

[2] G. J. Foschini and M. J. Gans, "On limits of wireless communications in a fading environment when using multiple antennas," *Wireless Personal Comm.*, Vol. 6, No. 3, March 1998, p. 311.

[3] A. Scaglione, D. L. Goeckel, J. N. Laneman, "Coopera-tive communications in mobile ad hoc networks, " *IEEE Signal Processing Magazine,* Vol. 23, No. 5, 2006, pp. 18-29.

[4] S. Jagannathan, H. Aghajan, A. Goldsmith, "The effect of time synchronization errors on the performance of cooperative MISO systems," *Proc. IEEE Globecom*, Dec. 2004, pp. 102-107.

[5] A. Özgür Yilmaz, "Cooperative Diversity in Carrier Frequency Offset," *IEEE Communications Letters*, Vol. 11, No. 4, April 2007, pp. 307-309.

[6] M. Schellmann, V. Jungnickel, "Effects of multiple users´ CFOs in OFDM-SDMA up-link – an interference model," *Proc. IEEE Int. Conf. on Communications (ICC 2006)*, Istanbul (TR), on CD-ROM.

[7] 3GPP TS 36.211 V1.20, *available:* www.3gpp.org.

[8] M. Schellmann, K. Manolakis, A. Ibing, M. Kuszak, "Impact of the Preamble Bandwidth on the Synchronization Performance," *Proc. 12th Int. OFDM-Workshop (InOWo)*, Hamburg, 2007.

[9] T. M. Schmidl and D. C. Cox, "Robust Frequency and Timing Synchronization for OFDM," *IEEE Trans. Commun.*, vol. 45, no. 12, pp. 1613_1621, Dec. 1997.

[10] M. Schellmann, "Improvements for Time and Frequency Synchronization in OFDM Systems," *Proc. 11th Int. OFDM-Workshop (InOWo)*, Hamburg, 2006.

[11] M. Kuszak, *Diploma Thesis*, TFH Berlin, 2006.

[12] M. Speth, S.A. Fechtel, G. Fock, H. Meyr, "Optimum Receiver Design for Wireless Broad-Band Systems Using OFDM—Part I,", *IEEE Trans. Commun.,* Vol. 47, No. 11, pp. 1668-1677.

[13] J. Bonnet, G. Auer, "Chunk-based Channel Estimation for Uplink OFDM," *Proc. 63rd IEEE VTC Spring,* 7-10 May 2006, Melbourne, Australia.

[14] S. Schiffermüller, V. Jungnickel, "Practical channel interpolation for OFDMA," *Proc. IEEE Globecom*, 2006, San Francisco, CA.

[15] V. Jungnickel, A. Forck, T. Haustein, C. Juchems, W. Zirwas, "Gigabit Mobile Communication using Realtime MIMO-OFDM Signal Processing", Chapter 11 *in MIMO System Technology for Wireless Communications*, ed. G. Tsoulos, Francis & Taylor 2006.

[16] G. Fettweis, E. Zimmermann, V. Jungnickel, E. A. Jorswieck, "Challenges in Future Short Range Wireless Systems," *IEEE Vehicular Technology Magazine*, Vol. 1, No. 2, 2007, pp. 24 – 31.

[17] S.D. Morgera, "Efficient synthesis and implementation of large discrete Fourier transforms," *SIAM Journal Comput*., Vol. 9, No. 2, pp. 251-272, 1980.

[18] *see:* www.rfel.com

[19] A. Ibing, V. Jungnickel, „On hardware implementation of multiuser multiplexing for SC-FDMA," submitted to IEEE VTC Fall 2007, Baltimore.

[20] V. Jungnickel, T. Hindelang, W. Zirwas, T. Haustein "SC-FDMA Waveform Design, Performance, Power Dynamics and Evolution to MIMO, " *Proc. IEEE Portable*, 25-27 March 2007, Orlando, FL.